# Chapter 7
# Luminescent Conjugated Polymer Dots for Biomedical Applications


**Guo Li, Tianshe Yang, Weiwei Zhao, Shujuan Liu, Wei Huang, and Qiang Zhao**

**Abstract** Luminescent conjugated polymer dots (CP-dots) have achieved significant progress in biomedical fields due to their excellent properties, such as excellent photophysical properties, good biocompatibility, tunable optical properties, and easy surface functionalization. In this chapter, recent advances on luminescent CP-dots for biomedical applications have been summarized, including their design strategy, preparation method, chemical structure, optical property, functionalization strategy, and biological applications. Importantly, their applications in biosensing, bioimaging, and disease therapy have been highlighted. Finally, the challenges and perspectives existing in the future development of luminescent CP-dots are also discussed.

**Keywords** Luminescent conjugated polymer dots · Biological detection · Biosensing · Bioimaging · Disease therapy

## 7.1 Introduction

Nanomaterials, as a class of important functional materials with one or more dimensions at the nanometer sizes of 0.1–100 nm, have attracted growing research interest in recent years. In comparison with their bulk counterparts [1–3], the nanoscale materials possess unique size-dependent optical and electronic properties [4, 5], due to their quantum size effect [6], surface effect [7], and macroscopic quantum tunneling effect [8], etc. These superior properties have endowed them potential applications in various fields including catalysis [9], chemical sensors [10],

G. Li · T. Yang · W. Zhao · S. Liu · W. Huang · Q. Zhao (✉)
Key Laboratory for Organic Electronics and Information Displays and Jiangsu Key Laboratory for Biosensors, Institute of Advanced Materials (IAM), Nanjing University of Posts and Telecommunications (NUPT), Nanjing, Jiangsu, P. R. China
e-mail: iamqzhao@njupt.edu.cn



X. Zhao, M. Lu (eds.), *Nanophotonics in Biomedical Engineering*,
https://doi.org/10.1007/978-981-15-6137-5_7

bioimaging [11], nonlinear optics [12], information storage [13], etc. In particular, luminescent nanomaterials have been widely studied since the beginning of research in nanomaterials. Recently, significant advances have been achieved for luminescent nanomaterials in the biomedical applications. There are mainly two types of luminescent nanomaterials, namely inorganic nanomaterials and organic nanomaterials, which are named after their compositions. Inorganic luminescent nanomaterials, including noble metal nanoclusters [14], carbon- or silicon-based nanomaterials [15, 16], and rare-earth-based nanophosphors [17], have been widely used in biomedical fields. Organic luminescent nanomaterials, especially those based on luminescent conjugated polymers (CPs) with π-delocalized backbones and fast electron transfer, have also enabled them wide applications in various biomedical fields, such as imaging, sensor, diagnosis, phototherapy, and photo-triggered drug delivery or release [18–21].

CPs, which are with the unique characteristics of delocalized electronic structures and organic π-conjugated backbones, show efficient coupling interactions among various optoelectronic segments [18, 20, 21]. Excitons can be effectively migrated to lower-energy electron/energy acceptor sites over long distances to quench the luminescence of CPs or to achieve the signal amplification of acceptors [18, 22–24]. Luminescent CP-dots have been widely applied in biomedical fields due to their unique properties, including excellent photophysical properties, good biocompatibility, tunable optical properties, and easy surface functionalization [18, 21]. These works focused on highly sensitive detection of disease-related biomarkers and diagnosis of pathogenic microorganisms [19]. Beyond sensing, optical imaging based on CP-dots, including near-infrared (NIR) luminescence imaging, time-resolved luminescence imaging (TRLI), and photoacoustic imaging (PAI) have also been successfully reported [25–28]. In addition, these nanomaterials have been applied in phototherapy, including photodynamic therapy (PDT) and photothermal therapy (PTT) [19, 28]. Moreover, anticancer therapy, gene delivery, multimodal therapy, drug delivery, and release are also included [19].

In this chapter, we summarize recent advances in luminescent CP-dots for biomedical applications, including their design strategy, preparation method, chemical structure, optical property, functionalization strategy, and biological applications. Especially, their applications in biosensing, bioimaging, and disease therapy have been highlighted. Finally, the challenges and perspectives existing in the future development of luminescent CP-dots are also discussed.

## 7.2 Advantages of Conjugated Polymer Dots for Biomedical Applications

CP-dots have been widely applied in the biomedical fields due to their unique properties, such as high brightness, superior photostability, excellent biocompatibility, tunable spectral property, and versatile surface modification. [18, 19]. Firstly, the

backbone structures of CP-dots can be properly regulated by introducing various components into the backbones and modifying the pendant chains with diverse recognition elements. Secondly, the fundamental photophysical property of CP-dots is easy to be tuned by changing their backbone structures. Thirdly, CP-dots can also offer stable hydrophobic backbones for the encapsulation and delivery of drugs, which can be monitored by the optical property of CP-dots. They also have the ability to be used as effective, protective, self-tracking, and stable carriers to transfer genes with decreased cytotoxicity in comparison with available transfection commercial reagents and no immune reaction compared to viral carriers [19, 29]. In addition, multifunctional CP-dots can be acquired through modifying various functional groups in order to achieve the integration of both detection and therapy [29].

## 7.3 Design, Synthesis, and Functionalization of Conjugated Polymer Dots

### *7.3.1 Structure and Category of CPs*

The design strategies for CPs focus on two main components, i.e., π-conjugated backbones and side chains, which constitute the major structures of the CPs. Firstly, the π-conjugated backbones have significant influence on the fundamental photophysical properties of CPs, such as the energy levels, charge transport properties, and luminescence quantum yields. The charged side chains, including carboxyl, sulfonic, phosphate groups and cationic quaternary ammonium groups, endow CPs the improved dispersibility in aqueous solution. Although numerous CPs have been developed during the past few decades, the basic backbone structures show no significant changes. According to the types of basic backbone structures, CPs can be divided into several categories, including poly(fluorene) (PF), poly(*p*-phenyleneethynylene) (PPE), poly(fluorene-co-phenylene) (PFP), poly(thiophene) (PT), poly(*p*-phenylenevinylene) (PPV), and their derivatives. The conventionally reported typical reactions for the preparations of CPs are shown in Scheme 7.1. All these backbones can be synthesized by classic organic reactions, such as Heck coupling reaction [30], Sonogashira coupling reaction [31], Suzuki coupling reaction [32], Wessling reaction [33], and $FeCl_3$ oxidative polymerization [34].

### *7.3.2 Preparation of CP-Dots*

In general, three typical methods are employed to prepare CP-dots, including miniemulsion, nanoprecipitation, and self-assembly methods (Scheme 7.2).

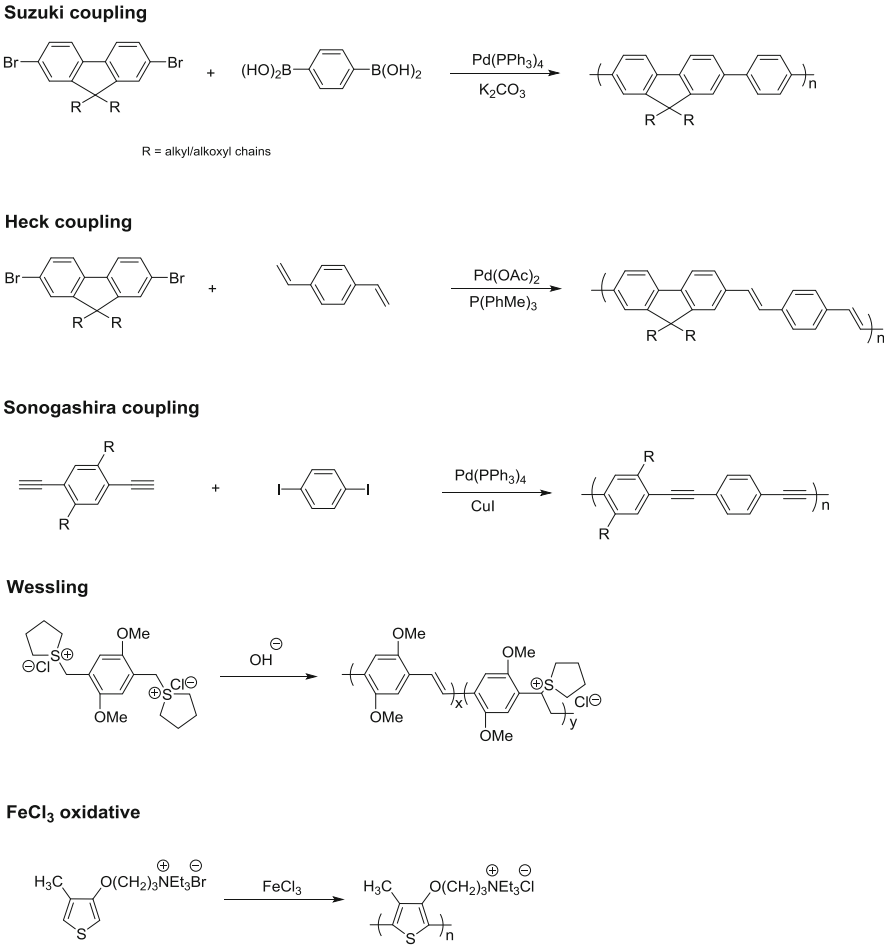


**Scheme 7.1** Typical polymerization methods for the preparation of CPs

### 7.3.2.1 Nanoprecipitation Method

In the nanoprecipitation approach, CPs are firstly dissolved in miscible solvents, such as acetonitrile and tetrahydrofuran (THF). Then, the as-prepared organic solution is quickly injected into a large amount of excess water under ultrasonication. The aggregation of CPs leads to the formation of CP-dots due to the improved hydrophobic interaction. Water-dispersible CP-dots can be obtained through removing the organic solvents by evaporation. Many reports have indicated that the particle diameters are highly determined by the starting CPs concentrations in organic solvent [35, 36]. As the concentration increases, the diameters of the CPs-dots become larger. In addition, the mixture of a polymer acceptor and a polymer donor is another route to prepare CP-dots with small sizes. Chiu et al.

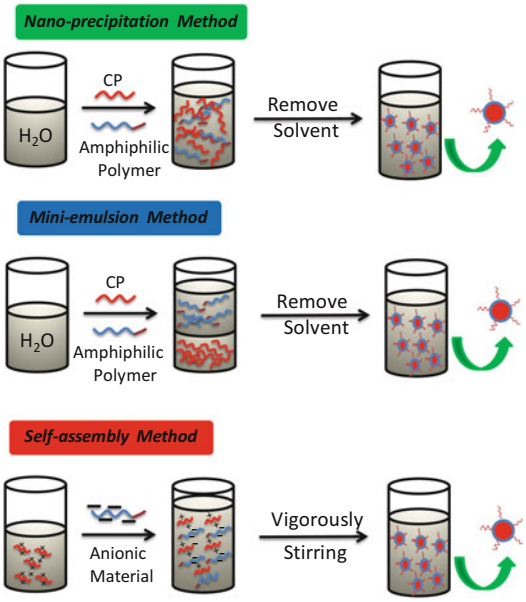


**Scheme 7.2** Schematic representation of three preparation methods of CP-dots

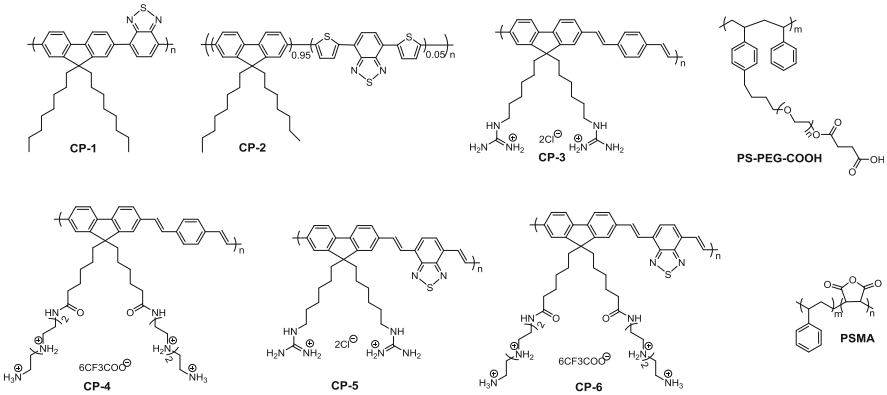


**Scheme 7.3** Chemical structures of **CP-1**, **CP-2**, **CP-3**, **CP-4**, **CP-5**, **CP-6**, PS-PEG-COOH, and PSMA

adopted amphiphilic poly(styrene-co-maleic anhydride) (PSMA) (Scheme 7.3) as carbonyl donors, **CP-1** or **CP-2** (Scheme 7.3) as polymer acceptor, and polymer matrices poly(styrene-g-ethylene oxide) (PS-PEG-COOH) (Scheme 7.3) as nano-encapsulated reagents to fabricate CP-dots through nanoprecipitation methods [37]. Dynamic light scattering measurement revealed that the acquired CP-dots exhibited an average diameter of ~15 nm in aqueous solution.

#### 7.3.2.2 Miniemulsion Method

In the miniemulsion approach, CPs or prepolymerized monomers are firstly dispersed in a nonpolar solvent. Then, the obtained solution is transferred into an aqueous solution containing surfactants to prevent the unwelcome coalescence of emulsion droplets. Under ultrasonication, the organic solution is mixed with the aqueous solution to further form a stable miniemulsion. After removing the organic solvents via evaporation, a stable dispersion of CP-dots can be obtained in aqueous solution. Employing the method, Mecking et al. synthesized poly-(arylene diethynylene) CP-dots through a step-by-step polymerization of the monomers under Glaser coupling condition [38]. By covalently bonding fluorene and perylene dyes, the CP-dots with tunable emission colors can be obtained by controlling intramolecular energy transfer. In comparison with CPs in a good solution, the absorption spectra of CP-dots exhibited blue-shift through the nanoprecipitation and miniemulsion methods, which was ascribed to the reduced conjugation length and constrictively collapsed and unordered conformation [39].

#### 7.3.2.3 Self-Assembly Method

In the self-assembly method, the oppositely charged CPs and co-assembling reagents are, respectively, dissolved in water. Then, the as-obtained dispersions are mixed together at a specific ratio under stirring. Finally, the functionalized CP-dots are precipitated through a high-speed centrifugation. For example, Wang et al. synthesized multifunctional CP-dots through the interaction of cationic CPs and anionic functional molecules (Scheme 7.4). The antibacterial CP-dots were fabricated through electrostatic interactions between a cationic porphyrin (TPPN, Scheme 7.4) and a water-dispersible polythiophene (**CP-9**, Scheme 7.4) [40]. To enhance the antitumor performance of CP-dots, they developed a self-assembly method by an integration of anionic chlorambucil and cationic pentathiophene (5T) (Scheme 7.4) [41]. In addition, Wang et al. synthesized bifunctional CP-dots for applications in imaging and drug delivery through assembling cationic **CP-7** and poly(L-glutamic acid) modified antitumor drug doxorubicin (PG-Dox) (Scheme 7.4). They have developed and demonstrated multifunctional CP-dots through applying electrostatic interaction between the positive **CP-8** and the negative disodium salt 3,3′-dithiodipropionic acid (SDPA) (Scheme 7.4) [42].

### *7.3.3 Functionalization of CP-Dots*

In order to achieve the desirable application of CP-dots in biomedical field, a variety of multifunctional CPs have been synthesized and the corresponding functional strategies have been explored. In 1986, Lowe et al. firstly utilized CPs as an

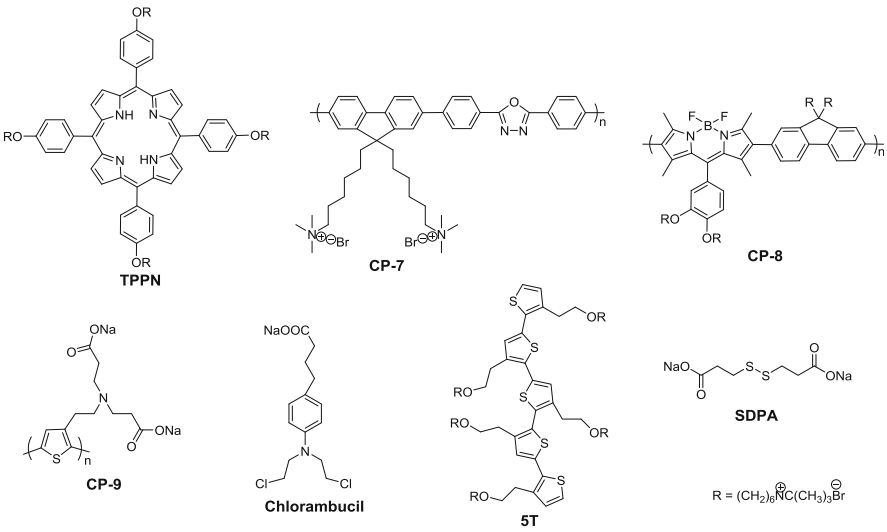


**Scheme 7.4** Chemical structures of TPPN, **CP-7**, **CP-8**, **CP-9**, chlorambucil, 5T, and SDPA

enzymatic responsive sensor [43]. After that, various functionalization strategies of CPs have been provided for biomedical applications. Herein, two versatile strategies are introduced.

#### 7.3.3.1 Functionalization on CPs Backbone

In the first strategy, highly efficient Förster resonance energy transfer (FRET) pairs, intramolecular donor–acceptor units and the extended π conjugated monomers can be introduced into the backbone, which can greatly change the photophysical property of the polymer and provide effective method for achieving excellent CP-dots. In addition, the specific functional groups, such as amino groups, alkoxyl chains, carboxyl groups, and targeted moiety, can also be introduced into the backbones of CPs (Scheme 7.5). To achieve functionalization of CP-dots, the monomers are covalently attached to functional groups followed by polymerization to acquire various functionalized CP-dots. To achieve the desired functionality, energy acceptor or targeted group have been introduced into CPs backbones. Through modifying the side chains, Wang et al. developed various emissive CP-dots (**CP-3**, **CP-4**, **CP-5,** and **CP-6**) (Scheme 7.3) through a nanoprecipitation method. From the point of structure, **CP-5** and **CP-6** have the same hydrophobic basic framework but various pendant chains. The absorption and emission spectra of **CP-4** and **CP-6** showed more red-shift than those of **CP-3** and **CP-5** for the reasons that the inter-chain aggregated and energy transfer of CPs happened among the backbones [44].

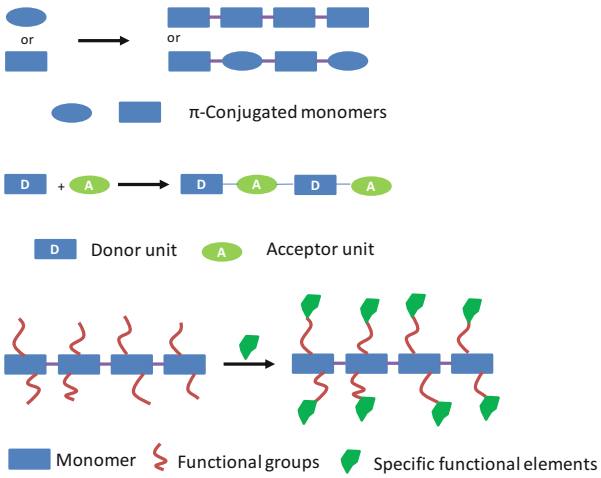


**Scheme 7.5** The modes and functionalization on CPs backbone

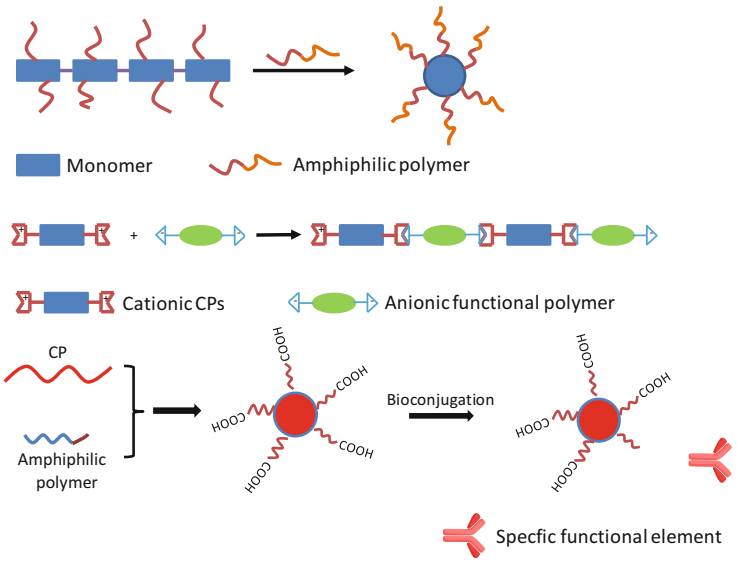


**Scheme 7.6** The modes and functionalization of CPs by self-assembly

### 7.3.3.2 Self-Assembly

In the self-assembly strategy, CPs themselves are functionalized through embedding recognition groups based on electrostatic or hydrophobic interactions (Scheme 7.6). Wang et al. synthesized multifunctional CP-dots through the self-assembly of cationic CPs and anionic functional molecules (Scheme 7.5). The functionalized

CP-dots were synthesized through electrostatic interactions between a water-dispersible cationic porphyrin (TPPN, Scheme 7.4) and anionic polythiophene (**CP-9**) (Scheme 7.4) [40]. They have synthesized four CPs with red, yellow, green, and blue emissions, and applied them as carboxyl functionalized CP-dots by a nanoprecipitation approach based on hydrophobic interactions between the CPs and poly(styrene-co-maleicanhydride) (PSMA) [25]. Another strategy is surface functionalization, which serves as an extension of the second method. The surface carboxyl or amino groups are firstly generated on the CP-dots using an amphiphilic polymer. Then, the functional elements (sugar protein) are grafted to the specific surface functional groups (-$NH_2$ or -COOH) by condensation reaction (Scheme 7.6). Based on the surface bioconjugation approach, Chiu et al. developed a universal strategy to prepare CP-dots and demonstrated their application in specific cellular targeting and biorthogonal labeling [37].

## 7.4 Biological Detection

Luminescent CP-dots are an important class of sensing materials for biological detection, which possess characteristic features of signal amplification and distinctive light-harvesting ability [18, 22]. Compared with the sensing materials based on small molecules, luminescent CP-dots show outstanding advantages of wide detection range, high sensitivity, and tunable spectral response characteristics [18, 21]. To date, a great number of CP-dots-based luminescent sensing materials used in biological detection adopt the typical fluorescence quenching response by electron-deficient analyte systems and photo-triggered electron transfer mechanism [19, 20].

The energy transfer inside the CP-dots or intra-particle energy transfer of CP-dots from the polymer donor to the dye acceptor can be influenced by the compact stacking structure and high content of fluorescence polymers. The efficient energy transfer can enhance the fluorescence brightness, adjust the emission color, and improve the photostability [29, 45–48, 51–53]. These advantages endow them important applications in sensing of analytes or external environment.

### *7.4.1 Ion Detection*

Ion detection plays an important role in the biomedical field. Many conventional fluorescent probes show turn off response through using the CPs emission quenching via electro-deficient analytes by photoinduced electron transfer (PET) mechanism [21, 29]. However, a turn-on fluorescent response of probes upon interacting with analytes is more desirable from the point of practical. In the case, the fluorescence of CPs-dots firstly decreases with the reversible coordination interaction between a quenching analyte and the organic π-conjugated polymer backbone. And then, a balance of the analyte-quencher complex is established.

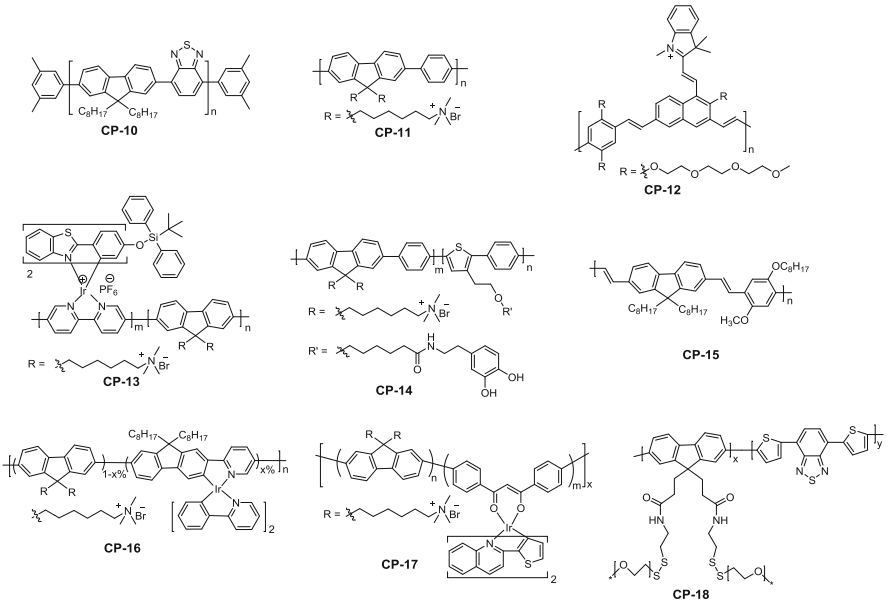


**Scheme 7.7** Conjugated polymers (**CP-10 ~ CP-18**) for biological detection

Finally, the emission of CP-dots recovers by a selective linkage of a target analyte with the quenching unit, which changes the balance toward the analyte-quencher complex [18, 21]. Moreover, a large number of nonfluorescent CP-dots are used as fluorescent probes for ion detection. They can display fluorescence nature after interacting with different analytes. Herein, the fluorescent detection of CP-dots for mercury ($Hg^{2+}$), calmodulin (CaM), hydrosulfide anions ($HS^{-}$) and fluoride ($F^{-}$) as examples are highlighted.

Mercury is a global pollutant in living organisms and environment due to its extreme toxicity. Fluorescence detection of $Hg^{2+}$ ions has become an important route to quantifying $Hg^{2+}$ concentration through the changes of the fluorescence intensity of the probes [21]. CP-dots have been reported as important fluorescent probes with low detection limit, wide detection range and quantitative analysis, especially for ultra-low $Hg^{2+}$ concentration. Harbron et al. synthesized fluorescent CP-dots through doping nonfluorescent rhodamine derivatives in **CP-10** (Scheme 7.7) and used them for the detection of $Hg^{2+}$ ions [45]. The as-prepared CP-dots emitted green-yellow fluorescence when the rhodamine derivatives on the nanoparticle surface contact $Hg^{2+}$ and then started to show orange-red fluorescence via FRET from the CP-dots to the rhodamine dyes. This signal amplification endowed the CP-dots to be responsive to $Hg^{2+}$ with low concentrations, in particular, in the range of 0.7–10 parts/billion.

CaM can regulate a variety of $Ca^{2+}$-dependent signal transductions and mediate activities of many proteins [46]. After $Ca^{2+}$-binding, the conformation of CaM from the closed form to the open one is observed, transferring to a clavate dumbbell-

shaped biomacromolecule. Accurate detection of CaM is essential for cellular activities, such as motility, secretion, and cell division. Wang et al. developed a hybrid CP-dots based on **CP-11** (Scheme 7.7) and graphene oxide (GO) for the detection of $Ca^{2+}$-triggered conformation changes of CaM by FRET mechanism [47]. In this hybrid system, the CaM was able to label the green fluorescent protein (EGFP). Upon $Ca^{2+}$-coordination, the conformation of CaM changed from the closed form to the open one. The excellent recyclable change towards the concentrations of $Ca^{2+}$ between 0 and $1.0 \times 10^{-3}$ M suggested that the assembly of EGFP-CaM with GO could be controlled by $Ca^{2+}$ reversibly and quantitatively. In addition, the transition of CaM is observed through the emission color changing under UV light excitation. This work revealed that hybrid CP-dots system showed excellent potential as diagnostic sensing materials for detecting $Ca^{2+}$-induced conformation changes in biological process.

Hydrosulfide anion is a key analyte, which attracts considerable attentions to develop various types of sensing materials due to the significance in industrial toxicity, pathology, human physiology, and biomedicine [48]. Fluorescent CP-dots-based sensing platform has the ability to monitor the low concentration of $HS^-$ anions in physiological media [49]. Nesterov et al. developed an effective turn-on amplifying fluorescent sensor based on CP-dots through introducing cyanine (as an analyte-specific unit) into the π-conjugated backbone (including the naphthalene fragment) of **CP-12** (Scheme 7.7) for the detection of $HS^-$ anions [50]. The specific reaction of $HS^-$ and the cyanine unit in CP-dots generated an efficient electronic insulation of the conjugated unit from the naphthalene fragment, thus causing significant enhancement of energy gap at this local site. This higher bandgap site diminished exciton migration length and caused the improved sensing performance of about tenfold higher detection sensitivity and a wide analyte detection region from nanomolar to millimolar. The signal amplification strategy can be further applied for designing a large number of other fluorescent sensing materials.

Fluorine ion is closely related to environmental and human dental health concerns [51]. It is of considerable interest to develop a novel probe that can accurately, rapidly, sensitively, and selectively detect $F^-$ ions in water and biomolecular process [51]. Zhao et al. developed ratiometric luminescence and lifetime probes based on CP-dots for the detection of $F^-$ ions [52]. They introduced *tert*-butyldiphenylsilyl (as a $F^-$-responsive unit) into red phosphorescent iridium(III) complex, which was linked to the main π-conjugated backbone of blue-emitting polyfluorene-based **CP-13** (Scheme 7.7). The fast response between CP-dots and $F^-$ can be achieved within 2 min. The ratios (the fluorescence intensity at 600 nm to that at 400 nm) of the CP-dots showed an excellent linear relation within the $F^-$ level from 5 to 13 μM. The CP-dots detection limit was measured to be 7.0 parts/billion, which was obviously lower than the recommended maximum limit of $F^-$ in practical drinking water.

### 7.4.2 pH Detection

pH is a key parameter in cellular and tissue homeostasis [53]. Therefore, it is of big significance to develop pH-responsive probe [54]. A turn-on pH sensing CP-dots platform can be achieved through linking a pH-response moiety to a CP. This platform is not involved in an aggregation effect but related to the property of pH-response moiety. The combination of pH-dependent property of pH-response moiety and the signal amplification features of CPs are expected to achieve a quick, acid-responsive, and sensitive pH sensor. For example, Wang et al. have reported a CP-dots-based pH assay probe, in which dopamine was covalently grafted to the side chain of a water-soluble **CP-14** (Scheme 7.7) [55]. The dopamine has various redox states, which can reversibly change between hydroquinone as reduced state and quinone as oxidized state in aqueous solution with the change of pH. At low pH, dopamine in its hydroquinone form shows strong fluorescence due to the missing electron transfer from the CPs backbone to hydroquinone. As pH increasing, the proportion of quinone structure of dopamine increases due to its auto-oxidation, therefore effective electron transfer from the CPs backbone to quinone generates and the emission of the CP-dots is quenched. The significant fluorescent response of CP-dots can be used to detect various pH.

### 7.4.3 Temperature Detection

Temperature is an important physical parameter in chemical or biological systems, which has significant influences on the equilibrium constants and biochemical reaction kinetics [56]. In general, CPs containing the temperature-sensitive moiety have the ability of temperature determination in cellular and tissue. Chiu et al. developed temperature-sensitive dye-rhodamine B (RhB)-attached CP-dots through a two-step process, in which RhB was first attached to polystyrene polymer (PS-$NH_2$) for PS-RhB, and then, PS-RhB and **CP-15** (Scheme 7.7) experienced nanoprecipitation process for the preparation of CP-dots [56]. The emission intensity of the as-synthesized CP-dots decreased with increasing temperature. It showed excellent temperature sensitivity (the liner range was 10–60 °C, $R^2 = 0.998$). Moreover, owing to the temperature insensitivity of **CP-15**, the as-prepared CP-dots could be applied in ratiometric temperature sensing under the excitation of a single wavelength (~450 nm) and possessing a linear range ($R^2 = 0.996$) for the temperature sensing, which well matched the physiologically relevant temperatures.

### 7.4.4 Biomolecule Detection

Accurately, sensitive and selective detection of ultralow levels of unique biomolecules is vital in early clinical diagnoses and therapy of diseases [57]. CP-dots, with a signal fluorophore doping in CPs, have been demonstrated to detect different biomolecules [19]. FRET-based mechanism has been widely used for biomolecule detection. The signal amplification effect of the backbone endows an excellent sensing ability to biomolecule analytes. Based on the typical FRET-based mechanism, one-step FRET process and two-step FRET process are mainly demonstrated. Moreover, two typical interactions, that is, chemical and physical interaction, between CPs and biomolecules, are mainly highlighted.

The one-step FRET process is the direct energy transfer from a single donor to acceptor. In the process, the interactions between CP-dots and analytes are mainly hydrophobic and electrostatic [19, 21]. For example, Huang et al. reported donor–acceptor (polyfluorene as donor and iridium(III) complex as acceptor) architecture **CP-16** (Scheme 7.7), which showed weak FRET responses toward proteins [58]. The hydrophobic interaction between proteins and CP-dots was able to break self-formed CPs aggregates, minimizing the FRET process. The emission ratio of $I_{430}/I_{605}$ of CP-dots showed good relationship in the region of 0–10 μM. The detection limit of the CP-dots was 0.006 μM. Furthermore, they synthesized water-soluble CP-dots containing iridium(III) complexes and polyfluorene and demonstrated their applications in time-resolved luminescent heparin detection [27]. The electrostatic interaction between **CP-17** (Scheme 7.7) and heparin triggers the CP-dots to be more compact, which was beneficial for improving the energy transfer from polyfluorene to iridium(III) complexes. The quantification range for heparin sensing was 0–70 μM in aqueous solution and 0–5 μM in serum, respectively. After addition of heparin, a 90-times maximum enhancement in the fluorescence ratio of $I_{632}/I_{430}$ of CP-dots was achieved.

Chemical interaction is another typical interaction between CP-dots and biomolecular, which have been applied in biomolecule detection [22, 29]. Huang et al. have developed **CP-18** (Scheme 7.7) with side disulfide linking to PEG chains [59]. The high-performance ratiometric probe was used as solubility-fluorescence changes for detecting thiol. A 12 times maximum enhancement in the fluorescence ratio of $I_{628}/I_{420}$ of CP-dots from 0.095 (without thiol) to 1.15 (with thiol) was found. According to the measurement results, the detection limit of the CP-dots was 0.021 mM. Owing to other cleavable-specific linkages can replace the disulfide, this design strategy can be extended as a versatile detection system for other analytes which can cleave the linkages.

Two-step FRET process affords many advantages, such as, higher-efficiency long-range energy transfer and more superior detection sensitivity for acceptor, than that of one-step FRET [60]. It is two parallel one-step energy transfers from a single donor to two different acceptors. Through the unique two-step FRET process, the detection sensitivity of CP-dots for adenosine deaminase (ADA) can be greatly improved. Guo et al. have developed this platform to monitor the enzymatic activity

of ADA [61]. In this system, an aptamer can be able to assemble into adenosine, causing ethidium bromide (EB) non-emissive, which was the final energy acceptor. The **CP-11** (Scheme 7.7) served as the energy donors, which could significantly enhance the emission of EB by a two-step FRET through adenosine transforming into inosine via ADA hydrolysis. At a region from 0 to 16 U/L of ADA, the enhancing ratio was linearly dependent on the level of ADA. The detection limit of ADA was measured to be 0.5 U/L. The ADA reaction time was 25 min, which was much more rapid and facile than that reported in literature [62, 63].

### *7.4.5 Hypoxia Detection*

Hypoxia, defined as oxygen-deprived condition, is a distinct feature of multifarious disease including tumors [64], stroke [65], and retinal disease [66]. Accurate hypoxia detection is not only very important for disease diagnosis, but also can be applied to evaluate therapeutic effects [67]. Phosphorescent transition-metal complexes (PTMCs)-based probes can be applied in fully reversible real-time monitoring of $O_2$ concentrations in vitro by employing the energy transfer between the triplet excited state of the metal complex and the triplet ground state of $O_2$ [68]. The CP-dots fabricated by introducing PTMCs into fluorescent CPs possessed the amplified signal output of CPs and the long emission lifetime of PTMCs, which endowed them excellent bio-probes for $O_2$ sensing.

Platinum(II) porphyrin complexes as an excellent class of $O_2$ sensor can be covalently attached into CPs backbone, and then the obtained CPs are self-assembled to form CP-dots in aqueous solution for oxygen detection [69]. For example, Zhao et al. developed dual-emissive **CP-19** and **CP-20** (Scheme 7.8) for oxygen detection through combining oxygen-responsive phosphorescent platinum (II) porphyrin into oxygen-insensitive polyfluorene backbone [69, 70]. Oxygen sensing mechanism of CP-dots is shown in Fig. 7.1. When the $O_2$ level decreased, the blue-emission intensity showed negligible change, while the red-emission intensity remarkably enhanced, revealing the phosphorescence sensitivity of Pt (II) porphyrin to $O_2$. The quantitative oxygen detection result of the two CPs was demonstrated through a good linearity equation. The $K_{sv}$ values were calculated to be $1.67 \times 10^{-2}$ $mmHg^{-1}$ for **CP-19** and $1.63 \times 10^{-2}$ $mmHg^{-1}$ for **CP-20**. The detection limit of the **CP-19** was 0.5 mmHg. Similarly, Papkovsky et al. adopted polyfluorene (**CP-21**) (Scheme 7.8) or poly(fluorene-alt-benzothiadiazole) as a FRET antenna and a fluorescent reference to covalently bond with metalloporphyrin and realized the quantitative $O_2$ imaging in a wide range of cell [71]. These CP-dots showed phosphorescence from Pt(II) porphyrin complex components with 5–10 times higher brightness and the improved two-photon cross section in comparison with the reported MM2 probes. In addition, the cell staining ability of these CP-dots could be adjusted with negatively and positively charged groups through grafting to the CPs. The zwitterionic CP-dots offered very high staining efficiency of live cells

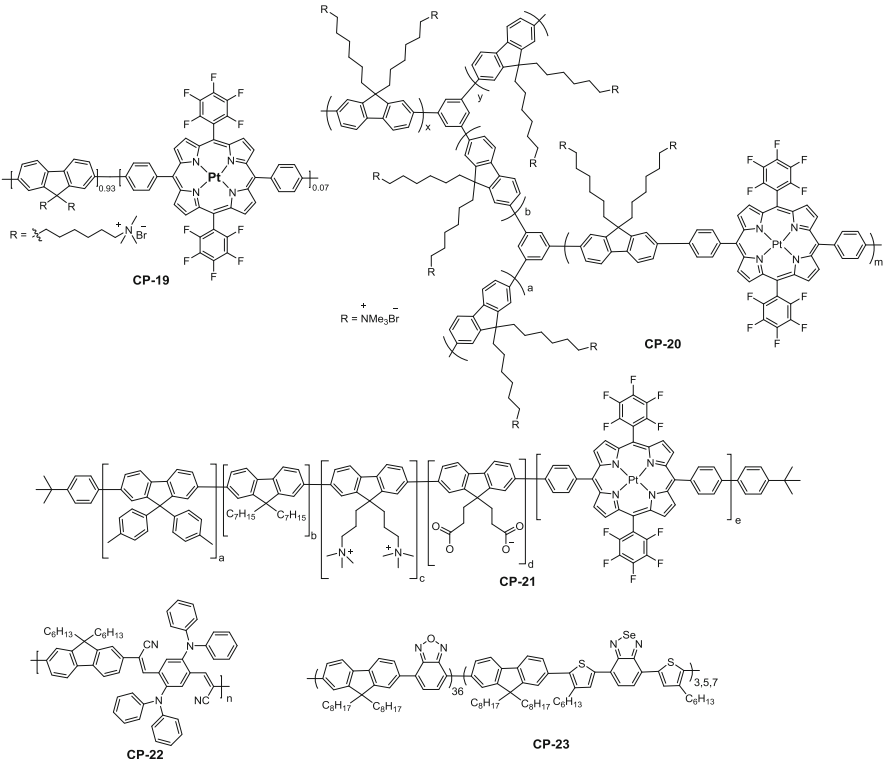


**Scheme 7.8** Conjugated polymers (**CP-19 ~ CP-23**) for biological detection

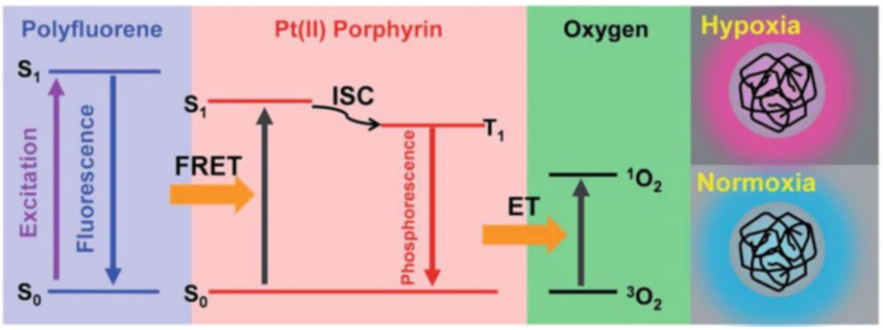


**Fig. 7.1** Oxygen sensing mechanism of CP-dots and schematic illustrations of the energy level of the moieties in CP-dots. (Reprinted with permission from Ref. [69]. Copyright 2015 Royal Society of Chemistry)

and spheroid cell models and could be applied to quantitatively detect $O_2$ via photoluminescence lifetime imaging microscopy (PLIM).

### *7.4.6 ROS Detection*

Reactive oxygen species (ROS) are considered as fundamental signaling members, which can regulate various biological species in a large number of physiological processes and associate with diverse pathophysiological processes, including autoimmunity, aging, and cancer diseases [72, 73]. Thus, developing probes to detect the generation of ROS is critical to both understanding the detailed effects of ROS in a large number of etiology-related diseases and well optimizing therapeutic interventions. Generally, CP-dots-based nanocomposites are designed by comprising a ROS-sensitive fluorophore unit (as the energy donor) and a ROS-inert core (as the energy acceptor), enabling the FRET from the donor to acceptor in the absence of ROS. The presence of ROS can decompose the energy fluorophore core of acceptor and subsequently disturb the FRET within the nanocomposites, ultimately causing an enhanced emission of the donor fluorophore unit.

One strategy is that a ROS-sensitive fluorophore unit is conjugated to the surface of CPs through nanoprecipitation methods. For example, Rao et al. have demonstrated a NIR CP-dots to detect reactive oxygen and nitrogen species (RONS) in inflammatory microenvironments in living mice [74]. The RONS-sensitive fluorophore unit (IR775COOH) was conjugated to the **CP-22** (Scheme 7.8) surface via a carbodiimide-activated coupling effect to generate CP-dots. The RONS could decompose the IR775COOH and then disturbing the FRET process within CP-dots, ultimately causing an increased fluorescence intensity of **CP-22**. The emission intensity ratio of $F/F_0$ ($F$ and $F_0$ stand for the fluorescence intensities at 678 nm in the presence and absence of RONS, respectively) changes showed a good linear relation to the levels of RONS in the ranges of 0–0.4 μM. The detection limit for the RONS was 10 nM in solution.

Another method is to incorporate the ROS-sensitive and -inert fluorophores into an all-in-one CPs to generate the nanoprobe. For instance, Chiu et al. reported a homogeneous fluorescent probe, which could be used for the ratiometric detection of hypochlorous acid [75]. In **CP-23** (Scheme 7.8), benzoxadiazole (OBT) acted as an energy donor and a $ClO^-$ sensitive unit, 4,7-bis(2-thienyl)-2,1,3-benzoselenadiazole (SeTBT) served as the energy acceptor, which enabled FRET from the OBT to the SeTBT without $ClO^-$. The CP-dots was prepared using PS-PEG-COOH and **CP-23** through a nanoprecipitation method. The $ClO^-$ could oxidize the fluorophore SeTBT and then inhibit the FRET process within CP-dots, ultimately causing an increased fluorescence of OBT in green channel and a decreased emission of SeTBT in NIR channel. The emission intensity ratio shifts showed a good linear relationship with $ClO^-$ levels in the ranges of 0–50 μM and 50–250 μM, respectively. The detection limit of the CP-dots for $ClO^-$ was 0.5 μM. The prepared homogeneous

probe could solve some problems of leakage or differential photobleaching when ratiometric measurements were carried out.

## 7.5 Biological Imaging

Due to the excellent optical properties and easy functionalization, CP-dots have been successfully applied in various biological imaging, including fluorescence imaging, time-resolved luminescence imaging, photoacoustic imaging, and multimodal imaging [18, 19, 29].

### *7.5.1 Fluorescence Imaging*

Fluorescence imaging technique has attracted growing attention due to their significant advantages of the availability of various biocompatible imaging agents, excellent temporal and spatial resolution and noninvasive nature [76]. Fluorescent CP-dots are developed as a desirable candidate in the fluorescence imaging application because of their excellent properties, such as excellent biocompatibility, superior photostability, high brightness, tunable spectral properties, and facile surface modification [18, 19, 29].

Conventional fluorescence imaging is considered as a kind of important optical imaging technique with the UV-vis emission region [77]. Many research results have demonstrated that CP-dots under the excitation of visible light display enhanced performance in the fluorescence imaging. Liu et al. have developed the integrated CP-dots nanocomposites through using gold nanoparticles (Au NPs) and CPs (**CP-24**, **CP-25**) (Scheme 7.9) by the miniemulsion approach [78, 79]. Au NPs acted as a powerful contrast agent in computed tomography and dark-field imaging due to the strong light scattering property from the localized surface plasma resonance. The fluorescence of CPs was well maintained in the nanocomposite due to the unique location of Au NPs. Therefore, the incorporation nanocomposite has been successfully used for fluorescence and dark-field dual-modal cellular imaging.

A multicolor CP-dots can be excited at various wavelengths, which well match with those available in commercial instruments used for fluorescence imaging [80]. Wang et al. firstly developed a new approach for constructing multicolor CP-dots-encoded (**CP-3 ~ CP-6**, Scheme 7.3) microparticles on the bases of noninvasive bacteria self-assembly [44]. A facile fabrication of multispectral microparticles has been achieved by bacteria-mediated assemblies of CP-dots for cell imaging. Furthermore, they developed four CPs (**CP-26 ~ CP-29**) (Scheme 7.9) with different emission colors and then applied them to synthesize carboxyl (-COOH) functionalized CP-dots through the nanoprecipitation approach with the hydrophobic interaction of the CPs and poly(styrene-co-maleicanhydride) (PSMA) [25]. The CP-dots functionalized with -COOH could also be developed through

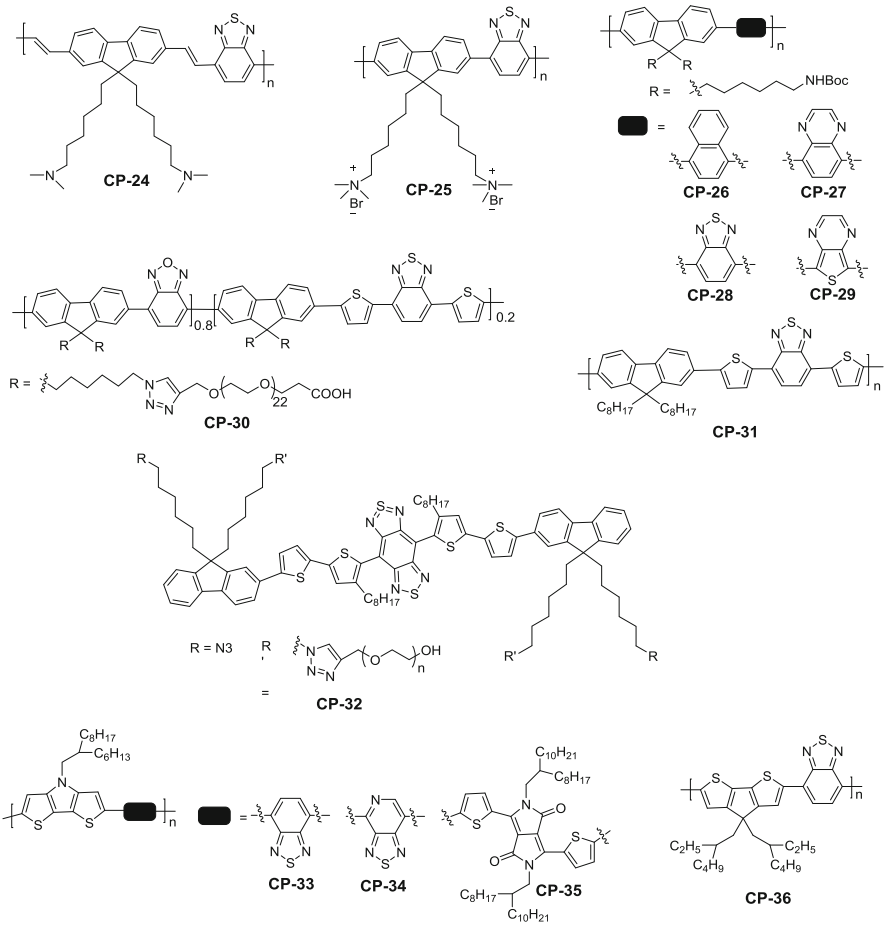


**Scheme 7.9** Conjugated polymers (**CP-24 ~ CP-36**) for fluorescence imaging

nanoprecipitation of four CPs with PSMA. Then, the acquired CP-dots were further modified with fundamental antibody for CP-dots-antibody conjugates. **CP-26 ~ CP-29**/PSMA CP-dots were modified by the antibody anti-EpCAM and used for MCF-7 cell imaging (Fig. 7.2a). As exhibited in Fig. 7.2b, multicolor fluorescence images of CP-dots were found under excitation at various wavelengths (405, 488 and 559 nm). Thus, the CP-dots could be excited by various wavelengths (405, 488 and 559 nm) that matched well to those available in commercial laser scanning confocal microscope applied for biosensor and biological imaging. Through binding each tumor cell to two CP-dots attached with various antibodies, much better specificity for targeted imaging and sensing was accomplished in comparison with single-antibody recognition form to tumor cells. The new approach has endowed multicolor CP-dots the ability for targeted imaging and other biological applications.

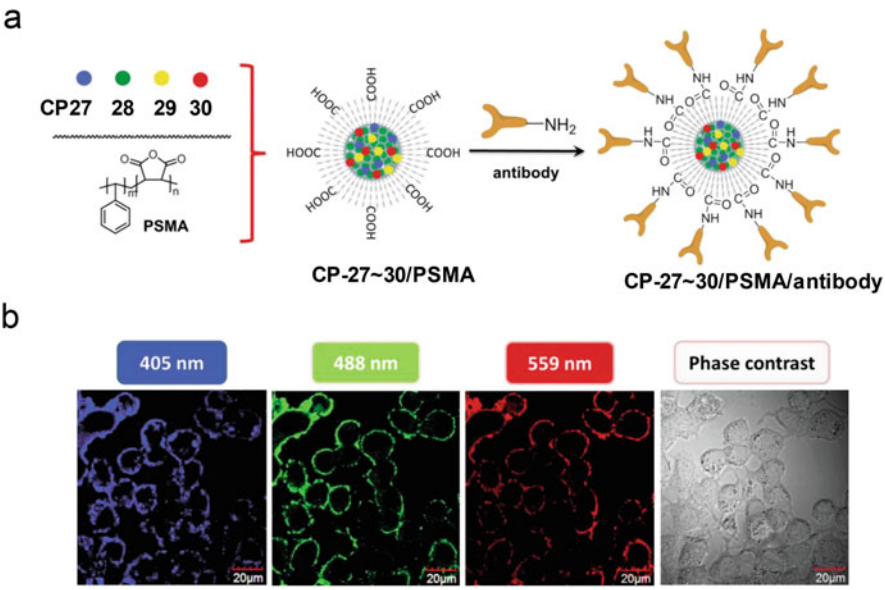


**Fig. 7.2** (**a**) The preparation of multicolor CP-dots (**CP-26 ~ CP-29**/PSMA) and their modification with an antibody. (**b**) Multichannel fluorescence images of MCF-7 cells with **CP-26 ~ CP-29**/PSMA/anti-EpCAM CP-dots. The excitation wavelengths are 405, 488, and 559 nm. (Reprinted with permission from Ref. [25]. Copyright 2014 Wiley-VCH)

In comparison with conventional fluorescence imaging, NIR fluorescence imaging is more desirable because the NIR region affords a particular interrogation window for biological applications with minimal interferential absorption, the deep penetration depth and low degree of scattering [81]. CP-dots offer a convenient approach for achieving NIR fluorescence by introducing the extended π conjugated monomers or the engineered donor–acceptor units into the backbone to lower the energy level.

Liu et al. have developed a bright NIR fluorescent **CP-30** (Scheme 7.9) with a high quantum yield of 25% and a large stokes shift of approximately 200 nm, which is suitable for cell imaging [82]. Phosphorylcholine with a zwitterionic molecular part, which is abundant onto the extracellular surface of the cell membrane, has been applied to decorate the **CP-31** (Scheme 7.9) surface by nanoprecipitation method [83]. The phosphorylcholine coating produces effective and rapid endocytosis and endows these CP-dots to enter cells within 30 min, and be clearly observed at 0.5 cm tissue penetration depth. The CP-dots are tolerant to physiologically ubiquitous ROS, generating durable emission both in vitro and in vivo.

Most recently, the imaging in the second NIR window (NIR-II, 1000–1700 nm) has attracted more and more research interest, because excellent fluorescence imaging performance can be obtained in this region, such as deeper penetration depth, superior temporal and spatial resolution, and higher signal/noise ratio (S/N) compared to the visible (400–750 nm) and NIR-I window (750–1000 nm) imaging

[84]. Dai et al. explored the molecular engineering on the donor unit through a shielding unit-donor-acceptor-donor-shielding unit structure, where benzobisthiadiazole (BBDT) serves as acceptor, thiophene serves as the donor and 9,9′-dialkyl substituted fluorene was employed as the shielding units [85]. The oligomer displays the optimum activity with fluorescence peaks centered at 1048 nm and a high QY of 5.3% in water. The high fluorescent performance of **CP-32** (Scheme 7.9) offers ultrafast (>25 frames/s) fluorescence imaging in the NIR-II window with superior spatial resolution. The S/N of imaging is 4.9 ± 0.3.

### *7.5.2 Time-Resolved Luminescence Imaging*

Time-resolved luminescence imaging is an effective way to distinguish the probe signals from background fluorescence or other luminophores with the similar emission wavelength [86]. TRLI technique mainly include time-gated luminescence imaging (TGL) and PLIM. In TGL method, the detector only collects the comparatively long-lived luminescence signals of the target probes and eliminates the unwanted short-lived background fluorescence through controlling the starting time for on-state of the detector, which considerably improves the detection accuracy and sensitivity [87, 88]. However, TGL method can only analyze the long-lived photon intensity over the gate time, which is usually used for the detection of analytes by long-lived probes. By contrast, PLIM can distinguish the lifetimes of every individual pixel and induce a significant alteration in the luminescence lifetime [89, 90]. The method can map lifetime spatial distribution in cells and tissues. To date, many CP-dots comprising of long-lived PTMCs and CPs with signal amplification nature have been reported as phosphorescent bioprobes for TRLI applications.

Zhao et al. have firstly reported a long-lived **CP-17**-based CP-dots (Scheme 7.7) containing polyfluorene units and phosphorescent Ir(III) complex and applied them for time-resolved luminescent heparin detection and photoluminescence lifetime imaging of KB cell membrane [27]. The phosphorescent turn-on **CP-17** probe for visual heparin sensor displayed high selectivity and quantification detection limit (0–70 μM and 0–5 μM in water and serum, respectively). The luminescence images suggested that the green emission was resulted from the short-lived background fluorescence, and the red emission was mainly assigned to the long-lived phosphorescence from CP-dots. TGL technique was adopted for heparin detection in complicated environment and in real patient blood samples, which clearly indicated the potential clinical application of the probe. The PLIM results indicated that the long-lived phosphorescent emission signals of **CP-17** CP-dots on the cell membrane could be differentiated from the short-lived background fluorescence. In a later work, a dual-emissive **CP-19** (Scheme 7.8) was synthesized by using polyfluorenes as an $O_2$-insensitive fluorophore and platinum(II) porphyrin as an $O_2$-sensitive phosphor, which could produce CP-dots in the aqueous solution owing to their amphiphilic structures [69]. Based on the sensitivity of long phosphorescence lifetime from Pt(II) porphyrins to oxygen, they used the CP-dots in TRLI of

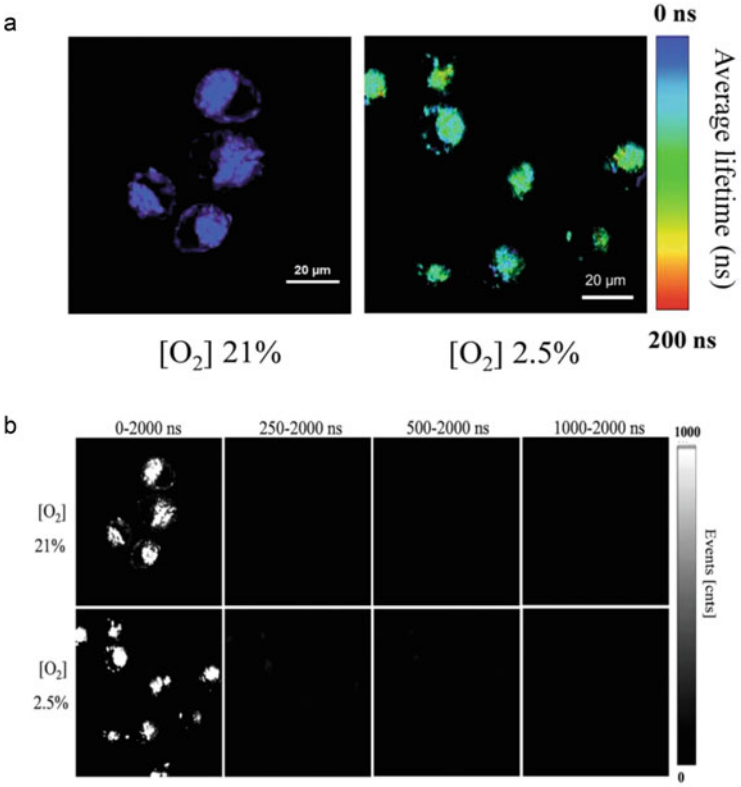


**Fig. 7.3** (**a**) Photoluminescence lifetime images ($\lambda_{ex}$ = 405 nm) of HepG2 cells incubated with 10 mg $mL^{-1}$ CP-dots at 37 °C for 2 h at $O_2$ concentrations of 21% and 2.5%, respectively. The magnification of the objective lens is 40×. The luminescence signals were collected in the range of 420–680 nm. (**b**) Time-gated luminescence intensity images ($\lambda_{ex}$ = 405 nm) of HepG2 cells incubated with the CP-dots (mg $mL^{-1}$) at 37 °C for 2 h at 21% or 2.5% $O_2$ with different time delays. The magnification of the objective lens is 40×. The luminescence signals were collected in the range of 420–680 nm. (Reprinted with permission from Ref. [69]. Copyright 2015 Royal Society of Chemistry)

intracellular oxygen concentrations. As shown in Fig. 7.3a, the emission lifetime was about 17 ns at 21% $O_2$ and enhanced to approximately 95 ns when the $O_2$ content decreased to 2.5%. The PLIM of intracellular $O_2$ concentration was achieved due to the relatively long average lifetime of CP-dots, in which the interference from short-lived background fluorescence was eliminated. TGLI technique accomplished highly sensitive $O_2$ sensing by collecting the signal at a long time range (250–2000 ns) (Fig. 7.3b). The research paved an avenue for the dual-emissive CP-dots to serve as TRLI bioprobes.

### 7.5.3 *Photoacoustic Imaging*

PAI detects phonon instead of photon under light irradiation and offers higher spatial resolution and deeper tissue penetration in comparison with the conventional optical spread range [91]. The PAI reagent should possess the characteristics of high photostability and large extinction coefficient at NIR range. CP-dots possessing strong NIR absorbance have been considered as a kind of promising candidates for PAI agent. They can be easily prepared by rational D-A structure control (intramolecular charge transfer) and systemically administrating organic nanoparticles (intra-particle molecular orbital engineering).

CP-dots with D-A structures have been widely applied in the fields of PAI. A higher D-A strength can lead to the stronger intramolecular charge transfer and lower band gap, which can further improve the photoacoustic signal [92]. Liu et al. synthesized three CP-dots comprising of CPs (**CP-33 ~ CP-35**) (Scheme 7.9) with D-A structures and DSPE-$PEG_{2000}$ as a matrix through nanoprecipitation method and applied them in PAI [93]. The extinction coefficient of **CP-35**-dots at 808 nm was 57.7 L $g^{-1}$ $cm^{-1}$, which was much larger than various reported PAI agents including $Cu_{2-x}Se$ NPs (8.5 L $g^{-1}$ $cm^{-1}$), $Bi_2Se_3$ nanosheets (11.5 L $g^{-1}$ $cm^{-1}$), PorCP (34.7 L $g^{-1}$ $cm^{-1}$), PFTTQ (3.6 L $g^{-1}$ $cm^{-1}$), and ICG (47.0 L $g^{-1}$ $cm^{-1}$), which suggested the strongest light harvesting ability of the **CP-35**-dots. The increased D-A strength of the corresponding CP-dots contributed to red-shifted absorption (703 nm for **CP-33**, 748 nm for **CP-34**, and 858 nm for **CP-35**), and inhibited fluorescence emission at 866 nm, 865 nm, and 885 nm with fluorescence QY of 3.2‰, 0.74‰, and 0.22‰, higher extinction coefficients of 55.0 L $g^{-1}$ $cm^{-1}$, 62.8 L $g^{-1}$ $cm^{-1}$, and 95.7 L $g^{-1}$ $cm^{-1}$, respectively, which caused improved photoacoustic signals. The photoacoustic measurement of **CP-35**-dots in tumor showed a high photoacoustic signal to background ratio of 47, which was superior to many reported photoacoustic contrast agents, such as ICG [94–97].

Intra-particle molecular orbital engineering strategy is another efficient route to prepare CP-dots for PAI. Pu et al. prepared CP-dots with amplified PAI brightness for new organic optical agents [28]. The doped CP-dots were synthesized by nanoprecipitation method using **CP-36** (Scheme 7.9) as the primary component and (6,6)-phenyl-C71-butyric acid methyl ester (PC70BM) as the secondary dopant. The molecular orbitals of the optical parts were aligned to endow the electron affinity and ionization potential of **CP-36**, which were higher than those of PC70BM. The energy level alignment favored PET within the confined system and caused quenched emission after light irradiation, which ultimately generated amplified PAI brightness (Fig. 7.4). The PAI brightness of the doped **CP-36**-dots was amplified 1.8-fold in the tumor in comparison with the nondoped CP-dots.

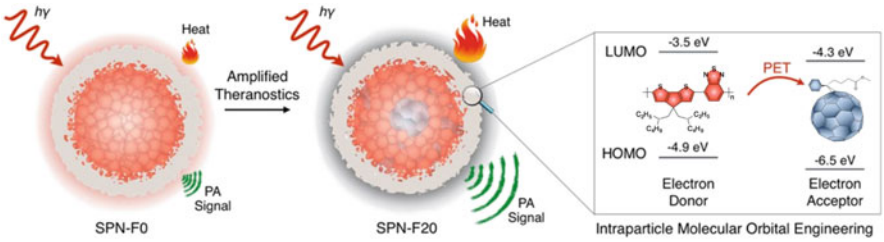


**Fig. 7.4** Illustration of PET-induced amplified theranostic **CP-36**. The highest occupied molecular orbital (HOMO) and lowest unoccupied molecular orbital (LUMO) are −4.9 and −3.5 eV for **CP-36** and −6.5 and −4.3 eV for PC70BM. (Reprinted with permission from Ref. [28]. Copyright 2016 American Chemical Society)

### *7.5.4 Multimodal Imaging*

Imaging modality generally contains optical imaging, TRLI, photoacoustic, computed tomography, magnetic resonance imaging (MRI), ultrasound, and positron emission tomography or single photon emission computed tomography [98]. Each imaging modality owns unique advantages along with intrinsic limitations, such as low spatial resolution, poor tissue penetration depth, high cost, and insufficient sensitivity. To achieve a better imaging performance, multimodal imaging, generally, dual modal or trimodal imaging, was developed. The combination of various imaging modalities is beneficial for overcoming obstacles existing in individual imaging, which can achieve higher spatial resolution, deeper penetration depth and more detailed biological information [99].

Liu et al. firstly reported the dual-modal imaging of iron oxides-based CP-dots including fluorescence imaging and MRI [100]. The CP-dots were prepared by encapsulating **CP-24** (as emission unit) (Scheme 7.9) and iron oxides (as magnetic domain) using a mixture of poly(lactic-co-glycolic-acid)-poly(ethylene glycol)-folate (PLGA-PEG-FOL) and PLGA through nanoprecipitation approach. They could serve as efficient bioprobes to accomplish targeting dual-modal imaging in vivo measurement. The signal intensity of MRI decreases with the increasing concentrations of **CP-24**, because **CP-24** could shorten the spin-spin relaxation time. The **CP-24**-dots containing iron oxides as bioprobes had superparamagnetic MRI with no reduced fluorescence intensity. The multimodal system based on CP-dots encapsulating different reagents with specific functionalities can provide great potential for in vivo bioimaging.

## 7.6 Therapy

Photo-induced tumor therapy usually contains two main types, such as PDT and PTT. In recent years, CP-dots have been reported as excellent therapeutic agents in phototherapy. They can be synthesized through grafting or encapsulating various photosensitizers and photothermal units into hydrophobic CPs backbone [19, 29].

### *7.6.1 Photodynamic Therapy*

As an emerging therapeutic modality, PDT possesses many advantages of noninvasive performance and highly efficient decreased disfigurement in comparison with conventional methods, such as surgery, chemotherapy, and radiotherapy [101]. It is usually composed of three components, i.e., photosensitizer (PS), molecular oxygen ($O_2$), and light. In PDT process, under proper wavelength irradiation, photosensitizer is activated to convert $O_2$ into cytotoxic ROS, which eradicates cancer cells. However, hypoxia in solid tumor microenvironment leads to low efficiency of PDT treatment. Some typical strategies have been explored to overcome tumor hypoxia, including in situ $O_2$ generation from endogenous $H_2O_2$ of tumor catalyzed by catalase or metal oxides, and direct $O_2$ delivering with endoperoxide, hemoglobin, calcium peroxide [101]. To date, many CP-dots-based therapeutic platforms have been established in PDT.

Considering the easy modification and versatile functionalization of CPs, CP-dots agents can be designed by integrating CPs with PS, catalase and bioactive molecules to meet the needs of various bioapplications for diagnosis and therapy. For example, some bioactive molecules, such as folic acid and peptides, have been grafted on the surface of CPs to achieve targeting CP-dots [19, 25, 29]. Wang et al. demonstrated an multifunctional CP-dots-based therapeutic platform, in which folic acid was aminated onto the surface of **CP-37** (Scheme 7.10), horseradish peroxidase (HRP) as oxygen-delivering unit was conjugated on a amphiphilic Janus dendrimer surface, and *meta-tetra*(hydroxyphenyl)-chlorin (m-THPC) acted as photosensitizer [102]. The CP-dots-based therapeutic platform could simultaneously achieve imaging and targeted PDT in tumors.

Besides grafting PS into CPs, some PS units can be designed in CPs backbone. Wang et al. described the design of **CP-38** (Scheme 7.10) containing polythiophene-porphyrin dyads and endowed concurrently PDT and imaging functions [103]. In **CP-38**-dots, energy was transferred from the polythiophene backbone to the porphyrin units under photoexcitation, which led to the generation of toxic singlet oxygen ($^1O_2$). PTMCs units can be introduced to CPs backbone or side chain, which offered phosphorescent CPs-dots with functions of phosphorescence and PSs. Huang et al. introduced phosphorescent Ir(III) complexes as PS to fluorene-contained **CP-39** (Scheme 7.10) via Suzuki coupling reaction, in which an efficient energy transfer was achieved from the main chain of **CP-39** to the Ir(III) complex

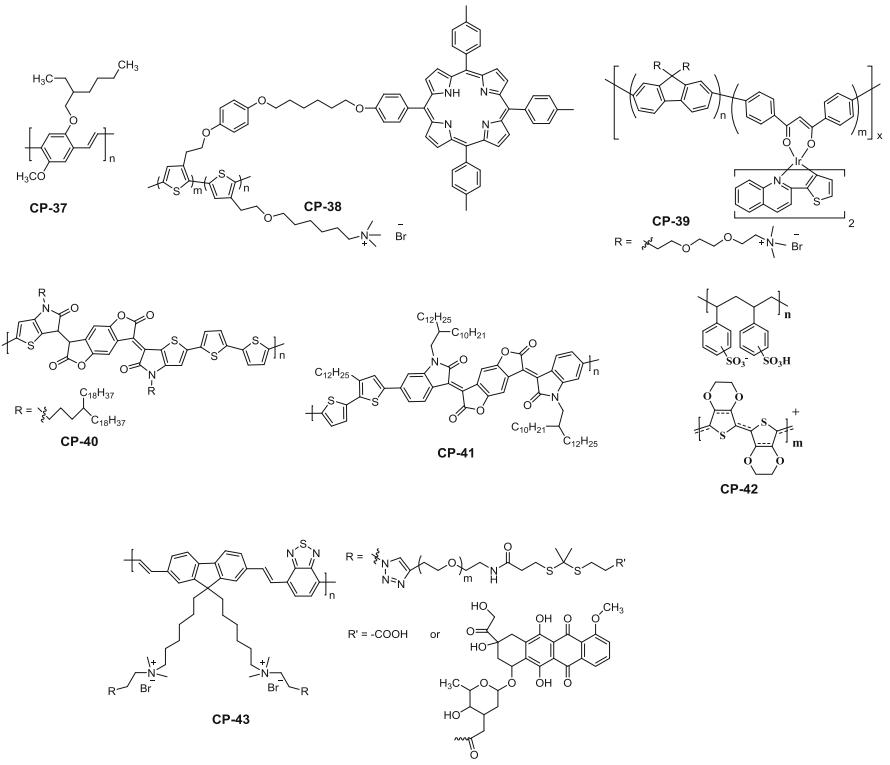


**Scheme 7.10** Conjugated polymers (**CP-37 ~ CP-43**) for therapy

[104]. In the PDT process, triplet-state oxygen was transferred into the singlet oxygen, which caused cellular damage, leading to the apoptosis and cell death (Fig. 7.5). In addition, Zhao et al. have also developed CP-dots based on the hyperbranched **CP-20** (Scheme 7.8) containing platinum(II) porphyrin as PS for PDT [70].

### *7.6.2 Photothermal Therapy*

PTT ablates tumor cells with localized heat, in which photothermal agents absorb NIR light and convert light energy into heat [105, 106]. It is highly selective and minimally invasive because PTT only happens at targeting sites and has good photothermal agent accumulations under concurrent NIR laser exposure [105, 107, 108]. In general, NIR organic dyes with strong NIR absorbance were adopted as photothermal agents; however, the photobleaching and hydrophobicity hinder their applications in PTT. In contrast, CP-dots with strong NIR absorption have unique

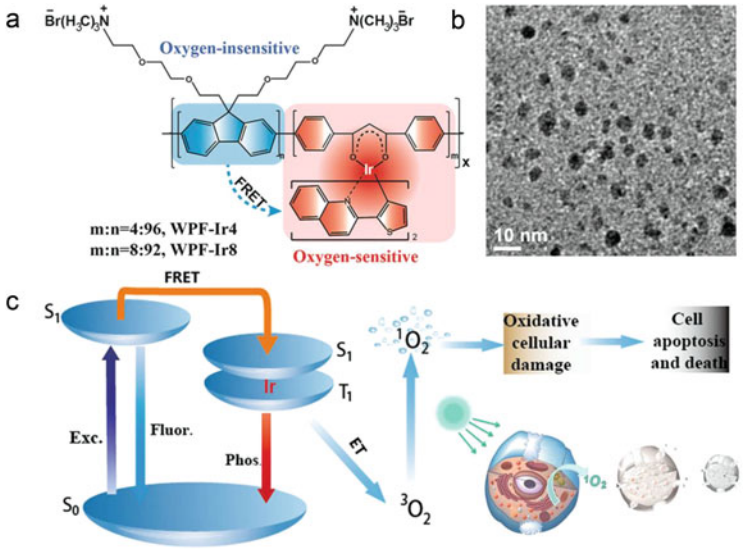


**Fig. 7.5** (**a**) Chemical structures of phosphorescent **CP-39** with the Ir(III) complex. (**b**) TEM of WPF-Ir4 in water. (**c**) Mechanism illustrating the oxygen sensing and PDT. (Reprinted with permission from Ref. [104]. Copyright 2014 Wiley-VCH)

advantages of good photostability, outstanding biocompatibility, large extinction coefficient, and favorable nonradiative exciton decay pathway to efficiently produce photothermal energy, which make them efficient PTT agents. The strategies for the preparations of CP-dots with strong NIR absorbance can be divided into two types, i.e., rationally designing molecular structure and systemically administrating organic nanoparticles.

CP-dots with an increased D-A strength possess enhanced red-shifted absorption and higher extinction coefficients, which have a positive effect on the PTT. As shown in Fig. 7.6, the CP-dots was formed based on CPs (**CP-33 ~ CP-35**) (Scheme 7.9) with D-A structure through a nanoprecipitation method [93]. The CP-dots with higher D-A strength had larger red-shifted absorption, faster photothermal heating, and highly efficient PTT in vitro and in vivo. In addition, Pu et al. developed an intraparticle molecular orbital engineering strategy to construct efficient CP-dots-based (**CP-36**) (Scheme 7.9) nanotheranostics with amplified PTT efficiency [28]. The temperature increase of the doped **CP-36**-dots was amplified 1.3-fold in the tumor in comparison with the nondoped CP-dots.

Recently, photothermal conversion in the second NIR optical window (NIR-II) has attracted considerable attention because it provides deeper tissue penetration and higher spatial resolution in phototherapy treatment [84, 85]. **CP-40**-dots (Scheme 7.10) with a narrow band gap has been reported as NIR-II photothermal materials, which own a high absorption coefficient of 39.5 L $g^{-1}$ $cm^{-1}$ (1064 nm) [109]. When used as photothermal nanoagents, it shows a high photothermal conversion efficiency of 50% and excellent imaging-guided PTT tumor treatment.

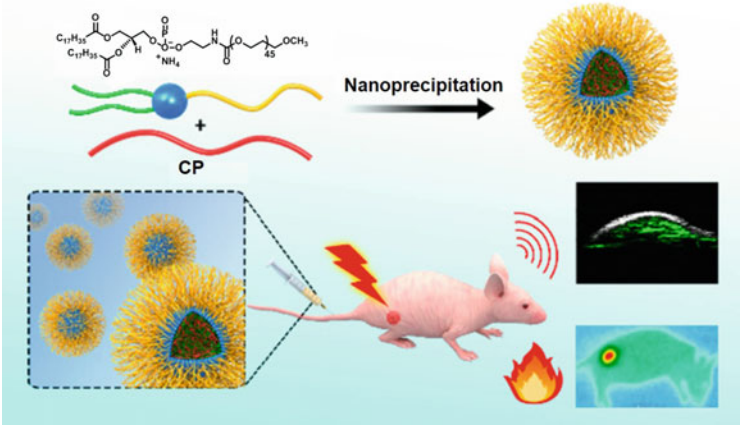


**Fig. 7.6** Illustration of the formation of **CP-35**-dots and photothermal performance in cancer theranostics. (Reprinted with permission from Ref. [93]. Copyright 2017 American Chemical Society)

### *7.6.3 Combined Therapy*

To achieve a better therapeutic performance, a combined therapy of PDT, PTT, chemotherapy, or radiotherapy has been reported [110, 112]. The combination of two or more therapeutic modalities facilitates combination of their advantages. The multifunctional CP-dots can be served as therapeutic agents for combined therapy. Their construction strategies are generally similar to the above-mentioned methods, including modifying the backbone or side chain of CPs, grafting or/and embedding specific functional units in CP-dots, and surface functional modification of CP-dots.

With D-A structures of a narrow band gap, CP-dots have been reported in the applications of PDT and PTT. Chen et al. first prepared D-A-type **CP-41** (Scheme 7.10) with 2,2-bithiophene as the donor and thiophene-fused benzodifurandione-based oligo(phenylenevinylene) as the acceptor [110]. The CP-dots were further fabricated from **CP-41** and poly(ethylene glycol)$_{114}$-*b*-poly(caprolactone)$_{60}$ (PEG-PCL) through a nanoprecipitation method. They realized highly efficient combined therapy of PDT and PTT because of the excellent photothermal conversion and singlet-to-triplet transition in the CPs with low bandgap.

In addition, CP-dots with the function of drug delivery can further improve the therapeutic efficacy of cancer. The drug carrier platform based on CP-dots can be established through loading multiple functional molecules including a water-soluble anti-cancer drug doxorubicin (DOX), a water-insoluble drug SN38 (a camptothecin derivative), or a photosensitizer chlorine 6 (Ce6) into PEDOT:PSS-PEG through π-π stacking and hydrophobic interaction. Liu et al. first synthesized PEDOT:PSS-PEG nanoparticles through the layer-by-layer assembly of commercial **CP-42** (Scheme 7.10) and PEGylation, and then loading them with three different therapeutic molecules (DOX, SN38, and Ce6) [111]. The CP-dots-based drug carriers can

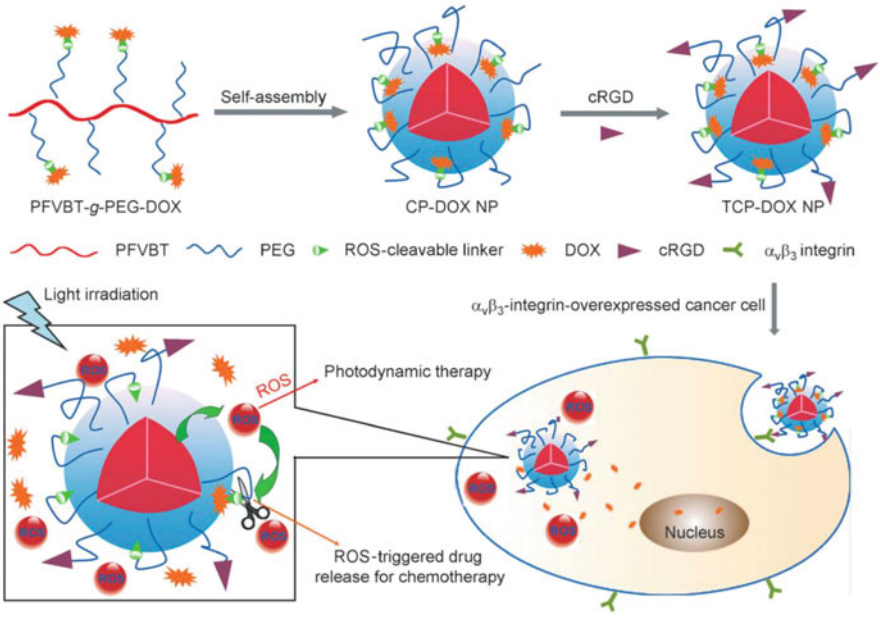


**Fig. 7.7** Schematic illustration of the light-regulated ROS-activated on-demand drug release and the combined chemo-photodynamic therapy. *PEG* poly (ethylene glycol). (Reprinted with permission from Ref. [112]. Copyright 2014 Wiley-VCH)

achieve drug delivery and combined therapy of PDT, PTT, and chemotherapy of cancer.

Besides loading drugs and delivery, drug release is a key factor to enhance therapeutic efficacy of cancer therapy. Liu et al. developed PEGylated **CP-43** (Scheme 7.10) as cancer-targeted nanocarriers, which can be applied for the combined therapy of chemotherapy and PDT (Fig. 7.7) [112]. Under single-light irradiation, the **CP-43**-dots acted as a PDT agent to generate ROS. At the same time, ROS could further activate drug release for chemotherapy. As a result, the combined therapy showed an enhanced therapeutic activity than the PDT or chemotherapy alone. The work provided an alternative approach to deliver and release encapsulated drugs and explored versatile theranostics with PDT and chemotherapy for tumor treatment.

## 7.7 Conclusion and Outlook

Luminescent CP-dots play a key role in biomedical applications because they exhibit several unique advantages, such as excellent photophysical properties, good biocompatibility, tunable optical properties, and easy surface functionalization. This chapter mainly summarizes recent progress on luminescent CP-dots for biomedical

applications, including their design strategies, preparation methods, and applications in biosensing, bioimaging, and therapy.

These CP-dots show high brightness, excellent photostability, good biocompatibility, and outstanding ability for sensing, imaging, and therapy. However, there still exists some drawbacks that hinder these CP-dots for more efficient biomedical applications. Firstly, it is rather difficult to acquire CP-dots with the uniform size through the as-reported preparation methods. Besides, although the existing CP-dots have possessed specific target functions in vivo, the specificity is rather low and the accumulation of CP-dots cannot be avoided in other organs and tissues. Lastly, from the views of practical applications, the innate metabolic processes and pathways of CP-dots in vivo are unclear so far. Therefore, more efforts should be made to solve the existing problems and investigate more significant and desirable performance through the design of new CP-dots. We sincerely hope that this chapter can inform readers about the current advancements of CP-dots from preparation to biomedical applications.

## References

1. Lu L, Shen Y, Chen X, et al. Ultrahigh strength and high electrical conductivity in copper. Science. 2004;304:422–6.
2. Alivisatos AP, Barbara PF, Castleman AW, et al. From molecules to materials: current trends and future directions. Adv Mater. 1998;10:1297–336.
3. Colvin VL. The potential environmental impact of engineered nanomaterials. Nat Biotechnol. 2003;21:1166–70.
4. Bruchez M Jr, Moronne M, Gin P, et al. Semiconductor nanocrystals as fluorescent biological labels. Science. 1998;281:2013–6.
5. Gu Y, Kuskovsky IL, Yin M, et al. Quantum confinement in ZnO nanorods. Appl Phys Lett. 2004;85:3833–5.
6. Goldstein AN, Echer CM, Alivisatos AP. Melting in semiconductor nanocrystals. Science. 1992;256:1425–7.
7. Ball P, Garwin L. Science at the atomic scale. Nature. 1992;355:761–6.
8. Reed MA, Frensley WR, Matyi RJ, et al. Realization of a threeterminal resonant tunneling device: the bipolar quantum resonant tunneling transistor. Appl Phys Lett. 1989;54:1034–6.
9. Corma A. From microporous to mesoporous molecular sieve materials and their use in catalysis. Chem Rev. 1997;97:2373–420.
10. Fan H, Lu Y, Stump A, et al. Rapid prototyping of patterned functional nanostructures. Nature. 2000;405:56–60.
11. Chan WCW, Nie S. Quantum dot bioconjugates for ultrasensitive nonisotopic detection. Science. 1998;281:2016–8.
12. Wang Y, Xie X, Goodson T. Enhanced third-order nonlinear optical properties in dendrimer-metal nanocomposites. Nano Lett. 2005;5:2379–84.
13. Service RF. Nanocrystals may give boost to data storage. Science. 2000;287:1902–3.
14. Chen LY, Wang CW, Zhi ZQ, et al. Fluorescent gold nanoclusters: recent advances in sensing and imaging. Anal Chem. 2015;87:216–29.
15. Zhu SJ, Tang SJ, Zhang JH, et al. Control the size and surface chemistry of graphene for the rising fluorescent materials. Chem Commun. 2012;48:4527–39.
16. Shen JH, Zhu YH, Yang XL, et al. Graphene quantum dots: emergent nanolights for bioimaging, sensors, catalysis and photovoltaic devices. Chem Commun. 2012;48:3686–99.

17. Peng JJ, Xu W, Teoh CL, et al. High-efficiency in vitro and in vivo detection of $Zn^{2+}$ by dye assembled upconversion nanoparticles. J Am Chem Soc. 2015;137:2336–42.
18. Feng X, Liu L, Wang S, et al. Water-soluble fluorescent conjugated polymers and their interactions with biomacromolecules for sensitive biosensors. Chem Soc Rev. 2010;39:2411–9.
19. Feng LH, Zhu CL, Yuan HX, et al. Conjugated polymer nanoparticles: preparation, properties, functionalization and biological applications. Chem Soc Rev. 2013;42:6620–33.
20. McQuade DT, Pullen AE, Swager TM. Conjugated polymer-based chemical sensors. Chem Rev. 2000;100:2537–74.
21. Thomas SW, Joly GD, Swager TM. Chemical sensors based on amplifying fluorescent conjugated polymers. Chem Rev. 2007;107:1339–86.
22. Swager TM. The molecular wire approach to sensory signal amplification. Acc Chem Res. 1998;31:201–7.
23. Dwight SJ, Gaylord BS, Hong JW, et al. Perturbation of fluorescence by nonspecific interactions between anionic poly(phenylenevinylene)s and proteins: implications for biosensors. J Am Chem Soc. 2004;126:16850–9.
24. Jiang YF, McNeill J. Light-harvesting and amplified energy transfer in conjugated polymer nanoparticles. Chem Rev. 2017;117:838–59.
25. Feng L, Liu L, Lv F, et al. Preparation and biofunctionalization of multicolor conjugated polymer nanoparticles for imaging and detection of tumor cells. Adv Mater. 2014;26:3926–30.
26. Ke CS, Fang CC, Yan JY, et al. Molecular engineering and design of semiconducting polymer dots with narrow-band, near-infrared emission for in vivo biological imaging. ACS Nano. 2017;11:3166–77.
27. Shi HF, Sun HB, Yang HR, et al. Cationic polyfluorenes with phosphorescent iridium(III) complexes for time-resolved luminescent biosensing and fluorescence lifetime imaging. Adv Funct Mater. 2013;23:3268–76.
28. Lyu Y, Fang Y, Miao QQ, et al. Intraparticle molecular orbital engineering of semiconducting polymer nanoparticles as amplified theranostics for in vivo photoacoustic imaging and photothermal therapy. ACS Nano. 2016;10:4472–81.
29. Wu CF, Chiu DT. Highly fluorescent semiconducting polymers dots for biology and medicine. Angew Chem Int Ed. 2013;52:2–26.
30. Bao ZN, Chen YM, Cai RB, et al. Conjugated liquid crystalline polymers-soluble and fusible poly(phenyleneviny1ene) by the heck coupling reaction. Macromolecules. 1993;26:5281–6.
31. Jiang JX, Su F, Trewin A, et al. Synthetic control of the pore dimension and surface area in conjugated microporous polymer and copolymer networks. J Am Chem Soc. 2008;130:7710–20.
32. Blouin N, Michaud A, Gendron D, et al. Toward a rational design of poly(2,7-carbazole) derivatives for solar cells. J Am Chem Soc. 2008;130:732–42.
33. Gowri R, Mandal D, Shivkumar B, et al. Synthesis of novel poly[(2,5-dimethoxy-p-phenylene)vinylene] precursors having two eliminatable groups: an approach for the control of conjugation length. Macromolecules. 1998;31:1819–26.
34. Liu B, Yu WL, Lai YH, et al. Synthesis, characterization, and structure-property relationship of novel fluorene-thiophene-based conjugated copolymers. Macromolecules. 2000;33:8945–52.
35. Kurokawa N, Yoshikawa H, Hirota N, et al. Size-dependent spectroscopic properties and thermochromic behavior in poly(substituted thiophene) nanoparticles. ChemPhysChem. 2004;5:1609–15.
36. Szymanski C, Wu CF, Hooper J, et al. Single molecule nanoparticles of the conjugated polymer MEH-PPV, preparation and characterization by near-field scanning optical microscopy. J Phys Chem B. 2005;109:8543–6.
37. Wu CF, Hansen SJ, Hou QO, et al. Design of highly emissive polymer dot bioconjugates for in vivo tumor targeting. Angew Chem Int Ed. 2011;50:3430–4.

38. Baier MC, Huber J, Mecking S. Fluorescent conjugated polymer nanoparticles by polymerization in miniemulsion. J Am Chem Soc. 2009;131:14267.
39. Pecher J, Mecking S. Nanoparticles from step-growth coordination polymerization. Macromolecules. 2007;40:7733–5.
40. Xing CF, Xu QL, Tang HW, et al. Conjugated polymer/porphyrin complexes for efficient energy transfer and improving light-activated antibacterial activity. J Am Chem Soc. 2009;131:13117–24.
41. Yang GM, Liu LB, Yang Q, et al. A multifunctional cationic pentathiophene: synthesis, organelle-selective imaging, and anticancer activity. Adv Funct Mater. 2012;22:736–43.
42. Chong H, Nie CY, Zhu CL, et al. Conjugated polymer nanoparticles for light-activated anticancer and antibacterial activity with imaging capability. Langmuir. 2012;28:2091–8.
43. Foulds NC, Lowe CR. Enzyme entrapment in electrically conducting polymers. J Chem Soc Faraday Trans. 1986;82:1259–64.
44. Feng XL, Yang GM, Liu LB, et al. A convenient preparation of multi-spectral microparticles by bacteria-mediated assemblies of conjugated polymer nanoparticles for cell imaging and barcoding. Adv Mater. 2012;24:637–41.
45. Childress ES, Roberts CA, Sherwood DY, et al. Ratiometric fluorescence detection of mercury ions in water by conjugated polymer nanoparticles. Anal Chem. 2012;84:1235–9.
46. Issihiki M, Anderson RGW. Function of caveolae in $Ca^{2+}$ entry and $Ca^{2+}$-dependent signal transduction. Traffic. 2003;4:717–23.
47. Yuan HB, Qi JJ, Xing CF, et al. Graphene-oxide-conjugated polymer hybrid materials for calmodulin sensing by using FRET strategy. Adv Funct Mater. 2015;25:4412–8.
48. Szabó C. Hydrogen sulphide and its therapeutic potential. Nat Rev Drug Discov. 2007;6:917–35.
49. Peng HJ, Cheng YF, Dai CF, et al. A fluorescent probe for fast and quantitative detection of hydrogen sulfide in blood. Angew Chem Int Ed. 2011;50:9672–5.
50. Chiang CH, Pangeni D, Nesterov EE. Higher energy gap control of fluorescence in conjugated polymers: turn-on amplifying chemosensor for hydrogen sulfide. Macromolecules. 2017;50:6961–6.
51. Kubik S. Anion recognition in water. Chem Soc Rev. 2010;39:3648–63.
52. Zhao Q, Zhang C, Liu S, et al. Dual-emissive polymer dots for rapid detection of fluoride in pure water and biological systems with improved reliability and accuracy. Sci Rep. 2015;5:16420.
53. Webb BA, Chimenti M, Jacobson MP, et al. Disregulated pH: a perfect storm for progression. Nat Rev Cancer. 2011;11:671–7.
54. Wang YG, Zhou KJ, Huang G, et al. A nanoparticle-based strategy for the imaging of a broad range of tumours by nonlinear amplification of microenvironment signals. Nat Mater. 2014;13:204–12.
55. Wen Q, Liu L, Yang Q, et al. Dopamine-modified cationic conjugated polymer as a new platform for pH sensing and autophagy imaging. Adv Funct Mater. 2013;23:764–9.
56. Ye FM, Wu CF, Jin YH, et al. Ratiometric temperature sensing with semiconducting polymer dots. J Am Chem Soc. 2011;133:8146–9.
57. Wang J. Nanomaterial-based amplified transduction of biomolecular interactions. Small. 2005;11:1036–43.
58. Sun P, Lu X, Fan Q, et al. Water-soluble iridium(III)-containing conjugated polyelectrolytes with weakened energy transfer properties for multicolor protein sensing applications. Macromolecules. 2011;44:8763–70.
59. Li J, Tian C, Yuan Y, et al. A water-soluble conjugated polymer with pendant disulfide linkages to PEG Chains: a highly efficient ratiometric probe with solubility-induced fluorescence conversion for thiol detection. Macromolecules. 2015;48:1017–25.
60. Watrob HM, Pan CP, Barkley MD. Two-step FRET as a structural tool. J Am Chem Soc. 2003;125:7336–43.

61. Wang C, Tang YL, Liu Y, et al. Water-soluble conjugated polymer as a platform for adenosine deaminase sensing based on fluorescence resonance energy transfer technique. Anal Chem. 2014;86:6433–8.
62. Zhang K, Yang QL, Zhang J, et al. An enzyme substrate binding aptamer complex based time-resolved fluorescence sensor for the adenosine deaminase detection. Biosens Bioelectron. 2013;42:87–92.
63. Zhang K, Wang K, Xie MH, et al. DNA-templated silver nanoclusters based label-free fluorescent molecular beacon for the detection of adenosine deaminase. Biosens Bioelectron. 2014;52:124–8.
64. Wilson WR, Hay MP. Targeting hypoxia in cancer therapy. Nat Rev Cancer. 2011;11:393–410.
65. Prass K, Scharff A, Ruscher K, et al. Hypoxia-induced stroke tolerance in the mouse is mediated by erythropoietin. Stroke. 2003;34:1981–6.
66. Frank RN. Diabetic retinopathy. N Engl J Med. 2004;350:48–58.
67. Zhang G, Palmer GM, Dewhirst MW, et al. A dual-emissive-materials design concept enables tumour hypoxia imaging. Nat Mater. 2009;8:747–51.
68. Papkovsky DB, Dmitriev RI. Biological detection by optical oxygen sensing. Chem Soc Rev. 2013;42:8700–32.
69. Zhao Q, Zhou X, Cao T, et al. Fluorescent/phosphorescent dual-emissive conjugated polymer dots for hypoxia bioimaging. Chem Sci. 2015;6:1825–31.
70. Zhou XB, Liang H, Jiang PF, et al. Multifunctional phosphorescent conjugated polymer dots for hypoxia imaging and photodynamic therapy of cancer cells. Adv Sci. 2016;3:1500155.
71. Dmitriev RI, Borisov SM, Duessmann H, et al. Versatile conjugated polymer nanoparticles for high-resolution $O_2$ imaging in cells and 3D tissue models. ACS Nano. 2015;9:5275–88.
72. Diehn M, Cho RW, Lobo NA, et al. Association of reactive oxygen species levels and radioresistance in cancer stem cells. Nature. 2009;458:780–3.
73. Dröge W. Free radicals in the physiological control of cell function. Physiol Rev. 2002;82:47–95.
74. Pu KY, Shuhendler AJ, Rao JH. Semiconducting polymer nanoprobe for in vivo imaging of reactive oxygen and nitrogen species. Angew Chem Int Ed. 2013;52:1–6.
75. Wu L, Wu IC, DuFort CC, et al. Photostable ratiometric pdot probe for in vitro and in vivo imaging of hypochlorous. J Am Chem Soc. 2017;139:6911–8.
76. Ntziachristos V, Bremer C, Weissleder R. Fluorescence imaging with near-infrared light: new technological advances that enable in vivo molecular imaging. Eur Radiol. 2003;13:195–208.
77. Grobe E, Calatayud A. Applications of chlorophyll fluorescence imaging technique in horticultural research. Sci Hortic. 2012;138:24–35.
78. Geng JL, Li K, Pu KY, et al. Conjugated polymer and gold nanoparticle co-loaded PLGA nanocomposites with eccentric internal nanostructure for dual-modal targeted cellular imaging. Small. 2012;8:2421–9.
79. Yuan YY, Ding D, Li K, et al. Tumor-responsive fluorescent light-up probe based on a gold nanoparticle/conjugated polyelectrolyte hybrid. Small. 2014;10:1967–75.
80. Bates M, Huang B, Dempsey GT, et al. Multicolor super-resolution imaging with photo-switchable fluorescent probes. Science. 2007;317:1749.
81. Frangioni JV. In vivo near-infrared fluorescence imaging. Curr Opin Chem Biol. 2003;7:626–34.
82. Liu J, Geng JL, Liu B. A bright far-red and near-infrared fluorescent conjugated polyelectrolyte with quantum yield reaching 25%. Chem Commun. 2013;49:1491–3.
83. Pu KY, Shuhendler AJ, Valta MP, et al. Phosphorylcholine-coated semiconducting polymer nanoparticles as rapid and efficient labeling agents for in vivo cell tracking. Adv Healthcare Mater. 2014;3:1292–129.
84. Hong GS, Zou YP, Antaris AL, et al. Ultrafast fluorescence imaging in vivo with conjugated polymer fluorophores in the second near-infrared window. Nat Commun. 2014;5:4206.

85. Yang QL, Hu ZB, Zhu SJ, et al. Donor engineering for NIR-II molecular fluorophores with enhanced fluorescent performance. J Am Chem Soc. 2018;140:1715–24.
86. Sun H, Liu S, Lin W, et al. Smart responsive phosphorescent materials for data recording and security protection. Nat Commun. 2014;5:3601.
87. Dai Z, Tian L, Song B, et al. Development of a novel lysosome-targetable timegated luminescence probe for ratiometric and luminescence lifetime detection of nitric oxide in vivo. Chem Sci. 2017;8:1969–76.
88. Connally RE, Piper JA. Time-gated luminescence microscopy. Ann N Y Acad Sci. 2008;1130:106–16.
89. Liu C, Wang XW, Zhou Y, et al. Timing and operating mode design for time-gated fluorescence lifetime imaging microscopy. Sci World J. 2013;2013:1–5.
90. Howard SS, Straub A, Horton NG, et al. Frequency-multiplexed in vivo multiphoton phosphorescence lifetime microscopy. Nat Photonics. 2013;7:33–7.
91. Wang LV. Multiscale photoacoustic microscopy and computed tomography. Nat Photonics. 2009;3:503–9.
92. Vezie MS, Few S, Meager I, et al. Exploring the origin of high optical absorption in conjugated polymers. Nat Mater. 2016;15:746–53.
93. Guo B, Sheng Z, Hu D, et al. Molecular engineering of conjugated polymers for biocompatible organic nanoparticles with highly efficient photoacoustic and photothermal performance in cancer theranostics. ACS Nano. 2017;11:10124–34.
94. Zhang SH, Sun CX, Zeng JF, et al. Ambient aqueous synthesis of ultrasmall PEGylated $Cu_{2-x}Se$ nanoparticles as a multifunctional theranostic agent for multimodal imaging guided photothermal therapy of cancer. Adv Mater. 2016;28:8927–36.
95. Qin H, Zhou T, Yang SH, et al. Fluorescence quenching nanoprobes dedicated to in vivo photoacoustic imaging and high-efficient tumor therapy in deep-seated tissue. Small. 2015;11:2675–86.
96. Xie HH, Li ZB, Sun ZB, et al. Metabolizable ultrathin $Bi_2Se_3$ nanosheets in imaging-guided photothermal therapy. Small. 2016;12:4136–45.
97. Pu KY, Mei JG, Jokerst JV, et al. Diketopyrrolopyrrole-based semiconducting polymer nanoparticles for in vivo photoacoustic imaging. Adv Mater. 2015;27:5184–90.
98. Lee DE, Koo H, Sun IC, et al. Multifunctional nanoparticles for multimodal imaging and theragnosis. Chem Soc Rev. 2012;41:2656–72.
99. Kim JY, Piao YZ, Hyeon T. Multifunctional nanostructured materials for multimodal imaging, and simultaneous imaging and therapy. Chem Soc Rev. 2009;38:372–90.
100. Li K, Ding D, Huo D, et al. Conjugated polymer based nanoparticles as dual-modal probes for targeted in vivo fluorescence and magnetic resonance imaging. Adv Funct Mater. 2012;22:3107–15.
101. Fan WP, Huang P, Chen XY. Overcoming the achilles' heel of photodynamic therapy. Chem Soc Rev. 2016;45:6488–519.
102. Zhang YR, Pang L, Ma C, et al. Small molecule-initiated light-activated semiconducting polymer dots: an integrated nanoplatform for targeted photodynamic therapy and imaging of cancer cells. Anal Chem. 2014;86:3092–9.
103. Xing CF, Liu LB, Tang HW, et al. Design guidelines for conjugated polymers with light-activated anticancer activity. Adv Funct Mater. 2011;21:4058–67.
104. Shi HF, Ma X, Zhao Q, et al. Ultrasmall phosphorescent polymer dots for ratiometric oxygen sensing and photodynamic cancer therapy. Adv Funct Mater. 2014;24:4823–30.
105. Lovell JF, Liu TW, Chen J, et al. Activatable photosensitizers for imaging and therapy. Chem Rev. 2010;110:2839–57.
106. Lovell JF, Jin CS, Huynh E, et al. Porphysome nanovesicles generated by porphyrin bilayers for use as multimodal biophotonic contrast agents. Nat Mater. 2011;10:324–32.
107. Jaque D, Maestro LM, Rosal B, et al. Nanoparticles for photothermal therapies. Nanoscale. 2014;6:9494–530.

108. Lyu Y, Zeng JF, Jiang YY, et al. Enhancing both biodegradability and efficacy of semiconducting polymer nanoparticles for photoacoustic imaging and photothermal therapy. ACS Nano. 2018;12:1801–10.
109. Sun TT, Dou JH, Liu S, et al. Second near-infrared conjugated polymer nanoparticles for photoacoustic imaging and photothermal therapy. ACS Appl Mater Interfaces. 2018;10:7919–26.
110. Yang T, Liu L, Deng Y, et al. Ultrastable near-infrared conjugated-polymer nanoparticles for dually photoactive tumor inhibition. Adv Mater. 2017;29:1700487–95.
111. Gong H, Cheng L, Xiang J, et al. Near-infrared absorbing polymeric nanoparticles as a versatile drug carrier for cancer combination therapy. Adv Funct Mater. 2013;23:6059–67.
112. Yuan YY, Liu J, Liu B. Conjugated-polyelectrolyte-based polyprodrug: targeted and image-guided photodynamic and chemotherapy with on-demand drug release upon irradiation with a single light source. Angew Chem Int Ed. 2014;53:7163–8.